AIAA JOURNAL
Vol. 33, No. 3, March 1995

Sound Generation by Flow over a Two-Dimensional Cavity

Jay C. Hardin*
NASA Langley Research Center, Hampton, Virginia 23681
and
D. Stuart Pope†
Lockheed Engineering and Sciences Company, Hampton, Virginia 23665

Sound generated by flow over a cavity at a Mach number of 0.1 and a Reynolds number based on cavity length of 5000 is calculated. The computation utilizes a two part technique where the time-dependent incompressible flow is first obtained and then a second calculation is performed for the compressible aspects of the flow. This second calculation utilizes a grid and numerical scheme designed for resolution of acoustic waves. The cavity flowfield is observed to oscillate quite regularly at the Strouhal number of 0.58 which produces an acoustic source of the same frequency. Time histories, spectra, and directivity of the sound radiation are computed.

Introduction

COMPUTATIONAL aeroacoustics (CAA) is rapidly emerging as a viable tool for understanding and reduction of aeroacoustic sources. The stringent requirements for such calculations have been thoroughly analyzed and numerical techniques have been validated through comparison with classical acoustic solutions. Unfortunately, however, these classical solutions are inviscid, and the sound is generated by surface motion, whereas most aeroacoustic sources are generated by the viscous dynamics of the fluid itself. Thus, the further development of computational aeroacoustics demands that CAA techniques be extended into this more complex arena.

The obvious approach to this problem is to utilize direct numerical simulation (DNS) where the compressible Navier–Stokes equations are solved to obtain the sound field radiated by a given viscous motion. However, a cursory analysis reveals that there are conflicting requirements for accurate calculation of both the viscous flow and the acoustic field which make such an approach extremely demanding computationally. In an attempt to overcome such obstacles, Hardin and Pope[1] proposed a two-part calculation where the viscous flow was first handled by calculating the time-dependent incompressible flow, and then the acoustic radiation was obtained from inviscid equations describing the differences from the incompressible flow. In this paper, this approach is applied to calculate the sound produced by viscous flow over a two-dimensional cavity.

Mathematical Formulation

Consider the geometry shown in Fig. 1. A flat surface contains a two-dimensional cavity of length L and depth D upstream of which exists a uniform subsonic inflow of velocity U_0 above a boundary-layer of height δ through which the velocity is reduced to zero at the surface. The vorticity dynamics associated with the cavity will produce a dipole-type sound radiation which should be more efficient than the quadrupole radiation in the incoming boundary layer. Define x as the streamwise and y as the cross-stream directions with origin at the center of the cavity floor (see Fig. 2) and incompressible velocity components U and V, respectively. Further, define the stream function $\psi(x, y, t)$ such that

$$U = \frac{\partial \psi}{\partial y} \qquad V = -\frac{\partial \psi}{\partial x}$$

and the vorticity

$$\Omega = \frac{\partial V}{\partial x} - \frac{\partial U}{\partial y}$$

Then the incompressible flow over the cavity may be computed from the stream function equation

$$\nabla^2 \Psi = -\Omega \tag{1}$$

and the Helmholtz equation

$$\frac{\mathrm{D}\Omega}{\mathrm{D}t} = \nu \nabla^2 \Omega \tag{2}$$

where ν is the kinematic viscosity of the fluid. After the stream function has been calculated, the incompressible pressure field may be obtained from the Poisson equation

$$\nabla^2 P = 2\rho_0 \left[\frac{\partial^2 \Psi}{\partial x^2} \frac{\partial^2 \Psi}{\partial y^2} - \left(\frac{\partial^2 \Psi}{\partial x \partial y} \right)^2 \right] \tag{3}$$

where ρ_0 is the constant incompressible density. However, as discussed in Ref. 1, incompressibility is only an approximation and, in fact, there are density fluctuations inherent in the incompressible flow which are larger than the acoustic density fluctuations of interest. These may be obtained by calculating the time-average pressure

$$\bar{P}(x, y) = \frac{1}{T} \int_0^T P(x, y, t)\, \mathrm{d}t$$

in the flow and supposing that fluctuations about this time-average pressure are isentropic. Here T is a time long compared to the period of any fluctuations in the flowfield. This leads to definition of a hydrodynamic density fluctuation

$$\rho_1(x, y, t) = \frac{P(x, y, t) - \bar{P}(x, y)}{c_0^2} \tag{4}$$

where c_0 is the ambient speed of sound in the medium, i.e., that which would be present if there were no flow. Solution of Eqs. (1–4) describes the essential viscous features of the flow.

The equations which actually describe the flow are the compressible Navier–Stokes equations. Suppose that the solutions to these

Received Oct. 23, 1993; revision received Oct. 5, 1994; accepted for publication Oct. 20, 1994.

*Chief Scientist, Acoustics Division.
†Principal Engineer, Acoustics and Dynamics Department. Member AIAA.

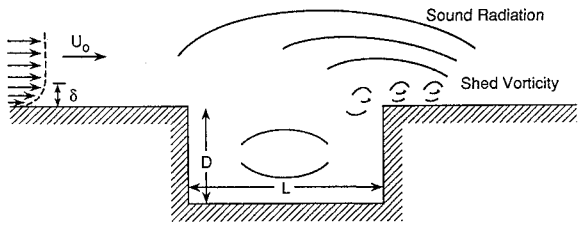

Fig. 1 Cavity geometry.

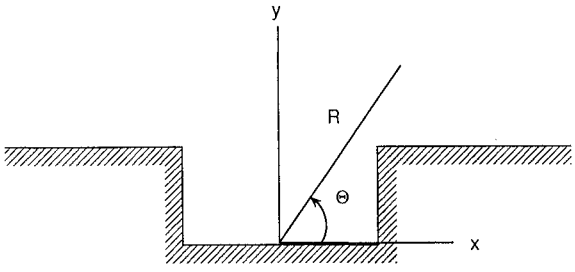

Fig. 2 Coordinate systems.

equations are written

$$\rho = \rho_0 + \rho_1 + \rho' \qquad u = U + u'$$

$$v = V + v' \qquad p = P + p'$$

where the primed variables are the differences between the compressible solutions and the corrected incompressible flow. If viscous action is assumed to have a negligible effect on these differences, they must satisfy the nonlinear inhomogeneous first-order partial differential equations

$$\frac{\partial \rho'}{\partial t} + \frac{\partial f_i}{\partial x_i} = -\frac{\partial \rho_1}{\partial t} - U_i \frac{\partial \rho_1}{\partial x_i}$$

$$\frac{\partial f_i}{\partial t} + \frac{\partial}{\partial x_j}[f_i(U_j + u_j') + (\rho_0 + \rho_1)U_i u_j' + p'\delta_{ij}]$$

$$= \frac{-\partial}{\partial t}(\rho_1 U_i) - U_j \frac{\partial}{\partial x_j}(\rho_1 U_i) \tag{5}$$

$$\frac{\partial p'}{\partial t} + c^2 \frac{\partial f_i}{\partial x_i} = -c^2 U_i \frac{\partial \rho_1}{\partial x_i}$$

where

$$f_i = (\rho_0 + \rho_1)u_i' + \rho'(U_i + u_i')$$

Also $c^2 = \gamma p/\rho$, γ is the ratio of specific heats in the fluid, $i = 1, 2$, and repeated subscripts are summed as per the Einstein convention.

Equation (5) is a set of four equations for the four unknowns u', v', p', and ρ' which contains the time-dependent incompressible solution as coefficients and forcing terms. If the incompressible flow were uniform, these would reduce to the Euler equations. Note that, although the fluctuations about the incompressible flow have been assumed isentropic, the background incompressible flow is viscous and dissipative. There are several advantages to this approach, the major being that optimum numerical schemes may be designed to handle both the viscous and the acoustic parts of the analysis.

Numerical Considerations

The incompressible flow given by Eqs. (1–3) is solved on a grid similar to that shown in Fig. 3. Here, lengths have been nondimensionalized by the cavity length L. A transformation is employed such that in the physical space, points are clustered along the walls to resolve the high-velocity gradients there, whereas in the computational domain, the grid is uniformly spaced. The flow is started with zero initial conditions, i.e.,

$$\psi(x, y, 0) = \Omega(x, y, 0) = 0$$

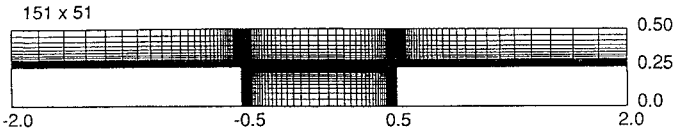

Fig. 3 Grid used in viscous calculations.

The boundary conditions include a specified quadratic inflow boundary-layer profile

$$U(x_i, y', t) = \begin{cases} \dfrac{U_0 y'}{\delta}(2 - y'/\delta) & 0 \le y' \le \delta \\ U_0 & y' > \delta \end{cases}$$

where x_i is the x coordinate of the inflow boundary, $y' = y - D$, U_0 is the incoming flow velocity, and δ is the height of the boundary layer. As will be shown, the cavity acoustic oscillation is sensitive to the incoming boundary layer. Thus, a more realistic assumption, preferably based on data, should be utilized to assure the correct boundary-layer instabilities. For the preceding simple profile

$$\Psi(x_i, y', t) = \begin{cases} \dfrac{U_0 y'^2}{\delta}(1 - y'/3\delta) & 0 \le y' \le \delta \\ U_0\delta(y'/\delta - 1/3) & y' > \delta \end{cases}$$

and

$$\Omega(x_i, y', t) = \begin{cases} \dfrac{-2U_0}{\delta}(1 - y'/\delta) & 0 \le y' \le \delta \\ 0 & y' > \delta \end{cases}$$

Along the walls, ψ wall $= 0$ and

$$\Omega \text{ wall} = \frac{-\partial^2 \psi}{\partial n^2}$$

where n is the direction normal to the wall. At outflow, the simple convective conditions,

$$\psi(x_0, y, t + \Delta t) = \psi(x_0 - \Delta x, y, t)$$

$$\Omega(x_0, y, t + \Delta t) = \Omega(x_0 - \Delta x, y, t)$$

where x_0 is the x coordinate at outflow, are implemented numerically. These conditions correspond to a frozen flow convecting at speed $\Delta x/\Delta t$, where Δx is the streamwise grid spacing at outflow and Δt is the time step. Finally, along the upper computational boundary, the simple conditions

$$\frac{\partial \psi}{\partial y}(x, y_m, t) = U_0 \qquad \Omega(x, y_m, t) = 0$$

where y_m is the y coordinate of the upper boundary, are employed.

For the incompressible solution, the Helmholtz equation, Eq. (2), is first stepped forward in time utilizing an explicit, second-order MacCormack[2] predictor/corrector technique and then the Poisson equation, Eq. (1), for the stream function is solved by successive over relaxation. This process is repeated until all initial transients have been eliminated and a steady-state flow is achieved.

Once the flow has stabilized, the incompressible pressure field is calculated from the Poisson equation, Eq. (3), in preparation for the acoustic computation. Dirichlet boundary conditions are first prescribed by setting the pressure in the upper left-hand corner of the computational domain to a constant value p_0 and then performing the line integral

$$P(x, y, t) = p_0 + \int_c \nabla P \bullet \partial \bar{c}$$

along the boundary. Here, ∇P is known from the momentum equations. Calculation of the pressure field is then accomplished by integrating Eq. (3) by successive over relaxation.

After the time-dependent incompressible field has been calculated, the acoustic field can be obtained through integration of

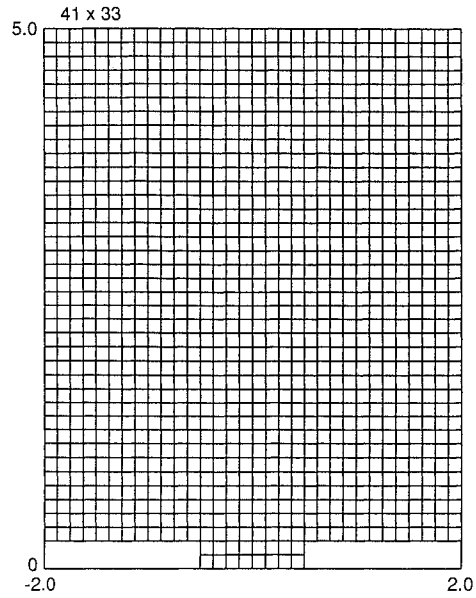

Fig. 4 Grid used in acoustic calculations.

Eqs. (5), again utilizing the MacCormack predictor-corrector technique. This is accomplished on a grid with uniform spacing Δ in both directions to minimize damping and dispersion of the acoustic waves. Experimental data[3] indicates that the cavity will oscillate with a characteristic frequency f corresponding to a Strouhal number on the order of

$$St = \frac{fL}{U_0} \simeq 1 \tag{6}$$

The acoustic waves produced will propagate at speeds between $c_0 - U_0$ and $c_0 + U_0$ depending on their direction. Thus, an estimate of the wavelength of the fundamental oscillation will be

$$\lambda = \frac{c_0}{f} \simeq \frac{L}{M_0}$$

on use of Eq. (6). Here, $M_0 = U_0/c_0$ is the Mach number of the flow. Therefore, the wavelength of the fundamental oscillation is larger than the cavity length in subsonic flows, indicating the disparity of scales which must be resolved in such problems. For this reason, the acoustic grid is taken much taller than the viscous grid, as shown in Fig. 4. Values of the incompressible variables above the viscous grid are assumed to be

$$U = U_0 \qquad V = 0 \qquad P = p_0$$

Although this grid appears very coarse for resolving the acoustic source, recent work by Lee and Koo,[4] utilizing the same acoustic/viscous splitting technique used here, showed good agreement with theory for sound generation by a spinning vortex pair even though the pair was spinning within one grid cell. Apparently this is due to the fact that the hydrodynamic density fluctuation falls off slowly with distance.

The cavity noise field will contain frequencies higher than the fundamental. Requiring N points per wavelength to adequately resolve the highest frequency of interest f_m yields

$$N = \lambda_m/\Delta$$

where $\lambda_m f_m = c_0$, which specifies the grid spacing of the uniform grid. Previous studies[5] have shown that something on the order of $N = 25$ is adequate for the second-order MacCormack scheme. Values of the incompressible solution are interpolated from the viscous grid onto the acoustic grid.

Finally, since the MacCormack scheme is the same order in both space and time,[2] dissipation and dispersion in this two-dimensional problem are then minimized by taking the Courant–Fredrichs–Lewy (CFL) number slightly less than

$$\frac{c_0(1+M)\Delta t}{\Delta} = \frac{1}{\sqrt{2}} \tag{7}$$

which then determines the time step for the acoustic calculation. As this time step is much larger than that required for the viscous, incompressible calculation, acoustic calculations are only performed after an appropriate number of viscous flow calculations.

Boundary conditions on the acoustic problem are somewhat more difficult due to the necessity of eliminating reflections of acoustic energy back into the computational domain. Of course, the normal component of the velocity fluctuation must be zero on the solid surfaces in addition to the incompressible normal velocity. Note that if $U_n = u'_n = 0$, where n indicates the direction normal to the wall, then $f_n = 0$ in Eq. (5) and the appropriate momentum equation yields

$$\frac{\partial p'}{\partial n} = 0$$

Further, it can be shown, in general, that

$$\frac{\partial p'}{\partial n} = c^2 \frac{\partial \rho'}{\partial n} + c^2 \frac{\partial \rho_1}{\partial n}$$

Thus, on the wall where $\partial p'/\partial n = 0$, it follows that

$$\frac{\partial \rho'}{\partial n} = -\frac{\partial \rho_1}{\partial n}$$

Finally, no boundary condition can be placed on the tangential velocity at the wall as that would overspecify the problem. Thus, the soft condition on the fluctuating tangential velocity at the wall needed by the numerical scheme is obtained by extrapolation from the interior.

Boundary conditions at the computational boundaries have been studied by several authors[6–8] on the basis of characteristic theory. This analysis indicates that, for subsonic flow, three characteristics must be specified at inflow boundaries and only one at an outflow boundary. Thus, at the inflow boundary $x = x_i$, the incoming entropy,

$$\frac{\partial p'}{\partial x} - c^2 \frac{\partial \rho'}{\partial x} = 0$$

the incoming vorticity,

$$\frac{\partial v'}{\partial x} - \frac{\partial u'}{\partial x} = 0$$

and the incoming acoustic wave

$$\frac{\partial p'}{\partial x} + \rho c \frac{\partial u'}{\partial x} = 0$$

are all nullified. At the upper boundary $y = y_m$, the incoming acoustic wave

$$\frac{\partial p'}{\partial y} - \rho c \frac{\partial v'}{\partial y} = 0$$

and at the outflow boundary, $x = x_0$, the incoming acoustic wave

$$\frac{\partial p'}{\partial x} - \rho c \frac{\partial u'}{\partial x} = 0 \tag{8}$$

are both nullified. These conditions are based on a linearized one-dimensional analysis. For example, in a uniform flow of velocity U_0, the outgoing acoustic wave will be of the form

$$u'(x,t) = f[x - (c_0 + U_0)t] \tag{9}$$

where $f(\cdot)$ is an arbitrary function and will satisfy the linearized momentum equation

$$\frac{\partial u'}{\partial t} + U_0 \frac{\partial u'}{\partial x} = -\frac{1}{\rho_0} \frac{\partial p'}{\partial x} \tag{10}$$

Thus, using Eq. (9) in Eq. (10), it can be seen that the outgoing wave will satisfy Eq. (8). On the other hand, the incoming wave will be of the form

$$u'(x,t) = g[x + (c_0 - U_0)t] \tag{11}$$

where $g(\cdot)$ is an arbitrary function and will satisfy the same momentum equation. Using Eq. (11) in Eq. (10), for this wave

$$c_0 \frac{\partial u'}{\partial x} = -\frac{1}{\rho_0}\frac{\partial p'}{\partial x}$$

and Eq. (8) will not be satisfied. Thus, this wave will be excluded.

Note also that by using Eq. (10), Eq. (8) could have been written in terms of time derivatives as

$$\frac{\partial u'}{\partial t} + (c + U_0)\frac{\partial u'}{\partial x} = 0$$

Implementation of these boundary conditions on the acoustic solution did not cause any obvious reflections from the boundaries, although small reflections are undoubtedly present due to their linearized, one-dimensional nature.

Other soft conditions needed by the numerics are obtained by extrapolation from the interior.

Initial conditions for the acoustic solution are obtained by noting that the primed quantities are the difference between the compressible and incompressible solutions. Thus, if compressibility is turned on at some initial time, the differences are

$$u' = v' = p' = 0 \qquad \rho' = -\rho_1$$

Results

The numerical technique described herein has been applied to a cavity with $L/D = 4$, $M_0 = 0.1$, $Re = U_0 L/\nu = 5000$, and $\delta = 0.1L$. The incompressible flow solution was first carried out to a nondimensional time of 88.75 with $\Delta t = 0.00025$ to assure that the steady-state flow had developed. Such a long calculation was not necessary but was done to demonstrate stability. Figure 5 depicts the incompressible vorticity field at a time after the flow has reached steady state. The steady state here consists of a vortex rolled up within the cavity which periodically entrains vorticity into the cavity and then ejects it out into the downstream wake.

Figure 6 is a plot of the nondimensional (by U_0 and L) vorticity as a function of nondimensional time as seen by an observer in the downstream wake of the cavity. Note that the waveform is quite periodic, oscillating with a period of 1.7 corresponding to a Strouhal number of 0.58. The classical understanding of this shear layer oscillation, which provides the forcing function for the cavity radiation, is that a vortex is shed from the leading edge of the cavity which convects at the convection speed U_c to the trailing edge.

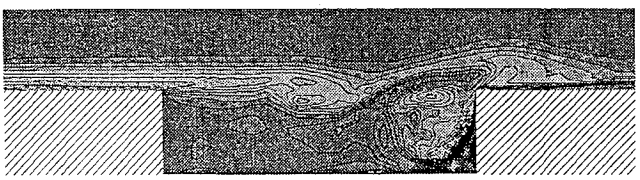

Fig. 5 Snapshot of incompressible vorticity field.

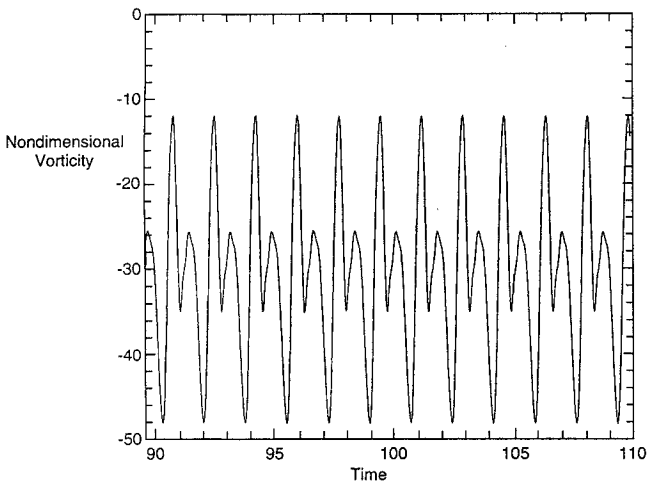

Fig. 6 Wake vorticity as a function of time.

There it causes an acoustic wave to be radiated which travels at the speed of sound back to the leading edge where it excites the shedding of the next vortex. Thus, the period of the fundamental oscillation is

$$T = \frac{L}{U_c} + \frac{L}{c_0} = \frac{L}{U_0}\left[\frac{U_0}{U_c} + M_0\right]$$

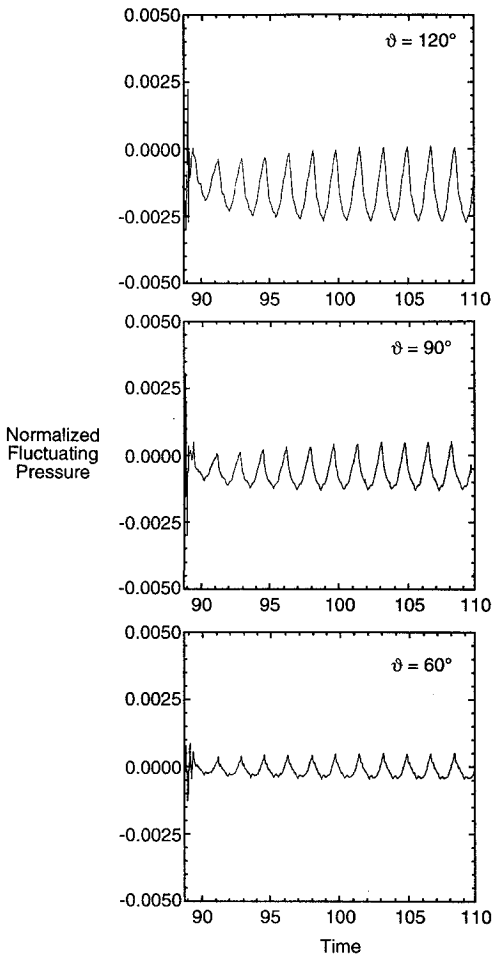

Fig. 7 Fluctuating pressure signal at various angles.

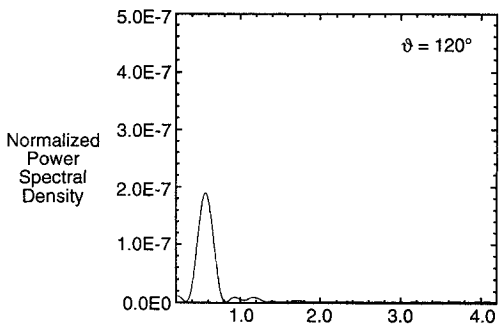

Fig. 8 Spectrum of pressure fluctuation.

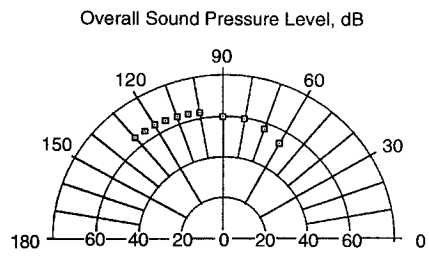

Fig. 9 Directivity pattern of cavity noise radiation.

or a Strouhal number of

$$St = \frac{fL}{U_0} = \frac{1}{[(U_0/U_c) + M_0]} \tag{12}$$

Multiples of this frequency are also possible depending on how many vortices are rolled up in the shear layer at once.

The present model, which solves for the incompressible field and then the acoustics, does not allow for any feedback of the acoustics on the flow. Thus, the acoustic half of the feedback loop presumably occurs at the infinite incompressible propagation speed rather than the speed of sound. Nevertheless, using the commonly accepted value of $U_c = 0.6U_0$, Eq. (12) yields $St = 0.57$ for the present case which is in good agreement with the numerical results. Neglecting the acoustic half of the feedback loop would predict $St = 0.6$. These values indicate that the cavity is oscillating in the $n = 1$ mode observed experimentally by Block[3] in her higher Reynolds number experiments.

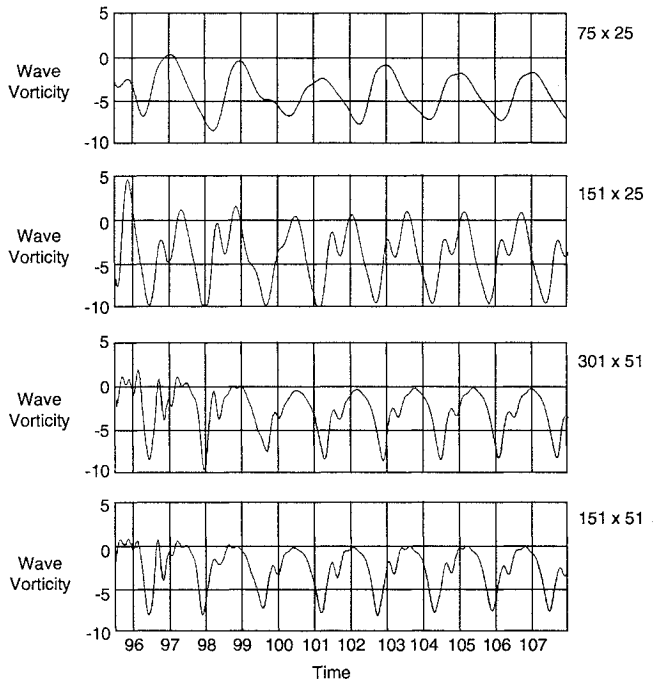

Fig. 10 Grid refinement studies.

After the incompressible flow had reached steady state, the acoustic calculation from Eq. (5) was initiated. This calculation utilized $\Delta t = 0.0625$ yielding a CFL number of 0.567. In the viscous calculation, the mean velocity $U_0$was used for nondimensionalization, whereas, in the acoustic calculation, the sound speed c_0 was employed. Thus, there were 25 viscous calculations between each acoustic calculation. The fluctuating pressure field was monitored at a distance of $R = 3L$ from the origin at the center of the floor of the cavity for several different angles $\theta(\theta = 0$ deg corresponds to downstream of the cavity, see Fig. 2). Figure 7 presents time history traces of the normalized fluctuating pressure p' at three of these angles. The acoustic computation was started at a nondimensional time of 88.75. After an initial transient, the acoustic signal becomes nearly periodic. Note that these waveforms have the sharp peaks and rounded troughs characteristic of nonlinear propagation. The small wiggles on these time traces are undoubtedly due to the use of the second-order MacCormack scheme and would disappear if a higher order scheme were implemented. The scales on the three plots of Fig. 7 are the same. Thus, it can be seen that the amplitude of the acoustic radiation increases with angle, indicating that the cavity is radiating preferentially in the upstream direction. Note also that the upper two of these curves have a small negative mean value. The reason for this is still under investigation, but does not indicate a numerical instability as calculations have been carried on for a further 10 nondimensional time units with the same stable periodic oscillation. It may be due to the fact that the observer is still in the near field of the source. Even $R = 3L$ is much less than a wavelength away at the fundamental frequency. A reviewer has suggested that it may be caused by the fact that nonlinear terms produce a component at zero frequency, e.g., $\cos^2 \omega t = \frac{1}{2} + \frac{1}{2} \cos 2\omega t$. Note that the mean value is largest where the pressure fluctuations are highest.

Figure 8 presents the power spectral density of the pressure fluctuation at the peak radiation angle of 120 deg as a function of Strouhal number. This spectral estimate has 10 degrees of freedom and a resolution of $\Delta St = 0.1$. Numerically, one faces the same problem that the experimentalist does, that of obtaining enough data for good resolution and low variability. All of the spectra had the same shape, exhibiting a peak near the fundamental Strouhal number 0.58 seen in the wake vorticity and very little power at Strouhal numbers greater than unity. Thus, the periodic pulsation of the cavity apparently leads to a periodic acoustic source in the flow.

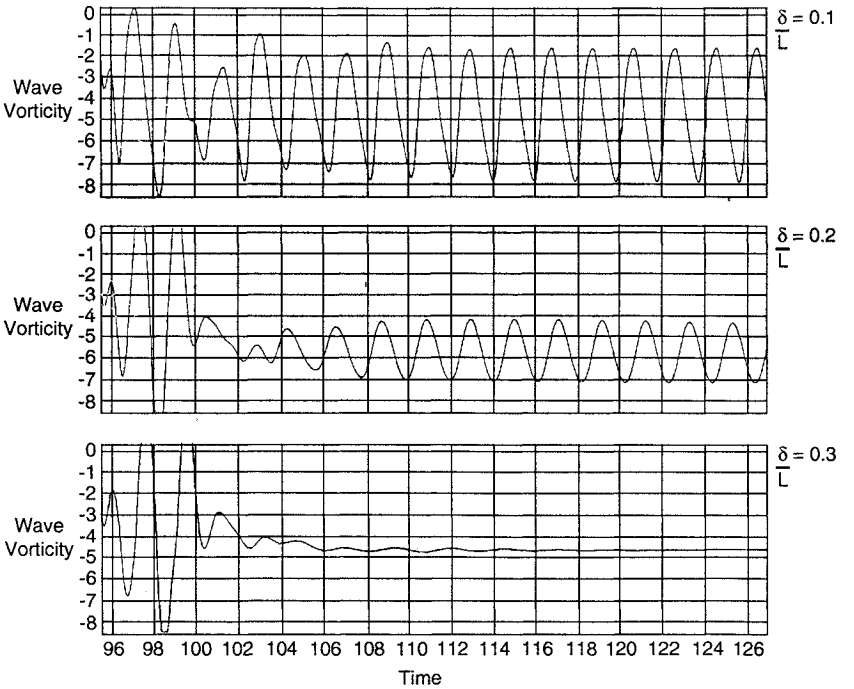

Fig. 11 Dependence of wake vorticity on boundary-layer thickness.

Finally, Fig. 9 presents the directivity pattern of the cavity noise radiation over the angular range 60 deg $\leq \theta <$ 130 deg which could be obtained on the acoustic grid. The levels ranged from 54 to 65 dB with peak radiation near the angle $\theta = 120$ deg. Although these results are predicted by a two-dimensional model, it can be shown that the acoustic levels radiated by a three-dimensional line source are essentially the same as those for a two-dimensional line source if the observer distance is less than the correlation length of the source region. Thus, these results should be valid for wide cavities.

To further validate these results, classical grid refinement studies were performed. Typical results are shown in Fig. 10 which displays the vorticity at a location one cavity length downstream of the cavity close to the surface. As there was very little difference between the calculations on the 151×51, 301×51, and 151×101 (not shown) grids, the 151×51 grid was deemed adequate to resolve the flow. The calculations, as might be expected, were more sensitive to transverse than to streamwise grid spacing. For grids on which the flow was resolved, small variations in the acoustic waveform could be observed, but the overall decibel level changed less than 1 dB from grid to grid, and the frequency content and directivity remained nearly invariant. Of course, the overall decibel level and, hence, directivity are basically controlled by the spectral peak in this case for which the Strouhal number was invariant. Such computations are fairly demanding. For example, calculations on the 151×101 grid required 32 h of CPU time and 6.8 Mbytes of storage on a Digital Equipment Corporation Alpha machine.

The numerical scheme has also been exercised to examine its dependence on various model parameters. The most sensitive parameter appears to be the boundary-layer thickness. Figure 11 displays calculations of the wake vorticity for three different boundary-layer thicknesses, $\delta/L = 0.1$, as used in the present study, as well as $\delta/L = 0.2$ and 0.3. Note that as the boundary-layer height is increased, the cavity response is reduced. This is due to the fact that the shear layer instabilities, which drive the cavity oscillation, are sensitively dependent on the boundary-layer velocity gradients.

Conclusions

This paper has presented a computational aeroacoustics calculation of sound generated by flow over a cavity. The technique utilized consisted of two parts: the time-dependent incompressible flow was first computed, and then a second calculation for the difference between the compressible and incompressible flow was accomplished. This technique was developed to optimize calculations of both the viscous and acoustic aspects of the flow. Because the acoustic grid was regular and coarse compared to the viscous grid, although covering a much larger area, each acoustic calculation took only one-fifth the time of each viscous calculation, and many viscous calculations were performed between each acoustic calculation. A direct numerical simulation with the same theoretical acoustic accuracy would require such a tiny regular grid and small time step that the cost would be prohibitive.

The computation demonstrated that the cavity flow undergoes a characteristic oscillation which leads to the radiation of sound. These oscillations, which were quite regular at the low-Reynolds number of the present numerical study, occurred at a Strouhal number which agreed with data taken at much higher Reynolds number. A sensitive dependence on boundary-layer height was also demonstrated. Although the present work merely demonstrates the feasibility of aeroacoustic calculations in viscous flows, this code is presently being modified in an attempt to increase the Mach and Reynolds numbers of the simulation to determine the velocity dependence of the source as well as to allow direct comparison with experimental data. In particular, a large eddy simulation (LES) approach which would compute only the larger scales while modeling the energy drain to the smaller scales is being incorporated to allow precise comparisons at higher Reynolds numbers.

References

[1]Hardin, J. C., and Pope, D. S., "A New Technique for Aerodynamic Noise Calculation," *Proceedings of the DGLR/AIAA 14th Aeroacoustics Conference*, AIAA, Washington, DC, 1992, pp. 448–456.

[2]MacCormack, R. W., "A Numerical Method for Solving the Equations of Compressible Viscous Flow," AIAA Paper 81-0110, Jan. 1981.

[3]Block, P. J. W., "Noise Response of Cavities of Varying Dimensions at Subsonic Speeds," NASA TND-8351, April 1976.

[4]Lee, D. J., and Koo, S. O., "Numerical Study of Sound Generation Due to a Spinning Vortex Pair," AIAA Paper 93-4370, Oct. 1993.

[5]Nark, D. M., "A Computational Aeroacoustics Approach to Sound Generation by Baffled Pistons," M.S. Thesis, George Washington Univ., Washington, DC, July 1992.

[6]Thompson, K. W., "Time Dependent Boundary Conditions for Hyperbolic Systems," *Journal of Computational Physics*, Vol. 68, Jan. 1987, pp. 1–24.

[7]Giles, M. B., "Non-Reflecting Boundary Conditions for Euler Equations," Massachusetts Inst. of Technology, Dept. of Aeronautics and Astronautics, TR CFDL-TR-88-1, Cambridge, MA, Feb. 1988.

[8]Colonius, T., Lele, S. K., and Moin, P., "Boundary Conditions for Direct Computation of Aerodynamic Sound Generation," *AIAA Journal*, Vol. 31, No. 9, 1993, pp. 1574–1582.